EXTERNAL CONTROL OF SATURN KILOMETRIC RADIATION

U. Taubenschuss[*], H. O. Rucker[*], W. S. Kurth[†], B. Cecconi[†], M. D. Desch[‡], P. Zarka[§], M. K. Dougherty[¶], and J. T. Steinberg[‖]

Abstract

The external control of Saturn kilometric radiation (SKR) by the solar wind has been investigated in the frame of the Linear Prediction Theory (LPT). The LPT establishes a linear filter function on the basis of correlations between input signals, i. e. time profiles for solar wind parameters, and output signals, i. e. time profiles for SKR intensity. Three different experiments onboard the Cassini spacecraft (RPWS, MAG and CAPS) yield appropriate data sets for compiling the various input and output signals. The time period investigated ranges from *DOY* 202 to 326, 2004 and is only limited due to limited availability of CAPS plasma data for the solar wind. During this time Cassini was positioned mainly on the morning side on its orbit around Saturn at low southern latitudes. Four basic solar wind quantities have been found to exert a clear influence on SKR. These quantities are: the solar wind bulk velocity, the solar wind ram pressure, the magnetic field strength of the interplanetary magnetic field and the y-component of the interplanetary magnetic field. All four inputs exhibit nearly the same level of efficiency for the linear prediction indicating that all four inputs are plausible drivers for triggering SKR. Furthermore, they act at completely different lag times ranging from $\sim 14\,h$ for the ram pressure to $\sim 52\,h$ for the bulk velocity. The lag time for the magnetic field strength is usually beyond $\sim 40\,h$ and the lag time for the y-component of the magnetic field is located around $\sim 30\,h$. So, an external influence from the solar wind is not directly converted into planetary radio energy but needs at least ~ 1.3 rotations of the planet to come into effect.

[*] *Space Research Institute, Austrian Academy of Sciences, Schmiedlstrasse 6, A-8042 Graz, Austria*
[†] *Dept. of Physics and Astronomy, University of Iowa, Iowa City, IA 52242, USA*
[‡] *NASA Goddard Space Flight Center, Greenbelt, MD, USA*
[§] *Observatoire de Paris, LESIA, UMR CNRS 8109, 92195 Meudon, France*
[¶] *Imperial College, Prince Consort Road, London SW7 2BW, UK*
[‖] *Los Alamos National Laboratory, Los Alamos, NM 87545, USA*

1 Introduction

The Saturn kilometric radiation (SKR) was detected for the first time when Voyager 1 was approaching Saturn in 1980 [Kaiser et al., 1980]. This nonthermal radio emission usually occurs in the frequency range 3 kHz - 1.2 MHz with a broad peak in flux density between 100 - 400 kHz [Kaiser et al., 1984]. Two components of opposite senses of nearly 100% circular polarization have been identified which propagate as X-mode waves. Radiation coming from the northern hemisphere is right-handed polarized (RH) and radiation coming from the southern hemisphere is left-handed polarized (LH). Similar to radio wave phenomena at Earth and Jupiter, the "Cyclotron Maser Instability" (CMI) is believed to be the primary driver for SKR generation [Wu and Lee, 1979]. The source regions are located in high magnetic northern and southern latitudes along auroral magnetic field lines which are centered around the noon meridian of Saturn. Studies performed by Galopeau et al. [1995] demonstrate that also source regions ranging down to 60° latitude on the morning and evening side are possible. UV observations of bright aurora phenomena performed with the Hubble Space Telescope confirm the presence of energetic auroral electrons in the morning-to-noon sector [Trauger et al., 1998]. Furthermore, SKR emission emitted from the nightside of Saturn has been reported recently by Farrell et al. [2005].
Correlation studies between variations of the solar wind and SKR emission have been performed by Desch [1982] for the first time. He found clear correlations between the solar wind ram pressure $\rho\, v^2$ (mass density ρ, bulk velocity v) and SKR intensity in Voyager 1 and 2 data sets. A further indication of the strong dependence of SKR activity on the solar wind was found by Kurth et al. [1983]. They detected a total disappearance of SKR during times when Saturn was moving through distant filaments of Jupiter's magnetotail and was thus shielded from the solar wind. Later on, Desch and Rucker [1983, 1985] improved those correlation studies also using the superposed epoch method as analysis tool and a compilation of various solar wind quantities. They came to the conclusion that besides the ram pressure also the solar wind momentum ($\rho\, v$) and the kinetic energy ($\rho\, v^3$) are significant drivers for triggering SKR. The highest correlation coefficients have been found at zero lag time with a time resolution of 10.66 hours, i. e. data have been integrated over one full rotation period of Saturn. The interplanetary magnetic field and its components revealed no clear correlation with SKR which may be due to the fact that solar wind measurements were performed up to 1.6 AU ahead of Saturn and had to be ballistically propagated to the point of the planet thereby ignoring hydrodynamic interactions of high- and low-speed streams inside the solar wind.
The solar wind exerts its external control not only on SKR generation but also on Saturn's aurorae as investigated recently by Clarke et al. [2005] and Crary et al. [2005]. New Cassini data in combination with ground-based and HST observations also enable to relate Saturn's radio emission phenomena to detailed auroral structures [Kurth et al., 2005].
The present paper re-analyzes the external control of SKR by the solar wind with the application of the Linear Prediction Theory, outlined in Chapter 2. The data used as input and output time series are described in Chapter 3 and the final Chapter 4 comprises the discussion and conclusion.

2 Basics of the Linear Prediction Theory

The starting point for the Linear Prediction Theory is the convolution equation. According to Wiener's approach for continuous functions it is defined as [Wiener, 1949]

$$Y(t) = \int_{-\infty}^{+\infty} f(s) \cdot X(t-s)\, ds \tag{1}$$

It says that the function $Y(t)$, called output signal, can be constructed by a convolution of another function $X(t)$, called input signal, and a filter function $f(s)$. t indicates the time and s is the temporal lag or temporal shift. Since we are dealing with discrete digital data rather than continuous analog functions, equation (1) has to be adapted to the discrete case:

$$Y_t = \sum_{s=-m}^{-1} f_s \cdot X_{t-s} \; + \; \sum_{s=0}^{M-1} f_s \cdot X_{t-s} \tag{2}$$

The filter f generates the output Y by weighting the input X by constants and then summing these weighted input data. The constants are called the filter coefficients f_s.
Note that the sum operator is already split into two sums, one over negative s-indices and one over positive s-indices. Splitting the sum operator separates the so-called "acausal" part of the filtering process (summation over negative s) from the causal part (summation over positive s).
The LPT uses the convolution equation outlined above in equation (2) to construct the filter coefficients f_s which are, at first, unknown. Therefore, not only a measured input signal X_t has to be given but also a measured output signal Z_t. The measured output is named Z_t in order to distinguish it from the calculated output Y_t. Besides the convolution equation, another condition is required. The mean-square-error between the calculated output Y_t and the measured output Z_t should be minimized in so far that Y_t becomes the best possible representation of Z_t. Stressing the convolution equation in combination with the statistical criteria of least squares fitting makes a calculation of the filter coefficients possible. The relationships between input, outputs and filter are sketched in Figure 1.

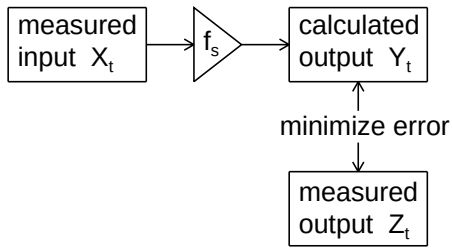

Figure 1: Schematics of the concepts of the Linear Prediction Theory.

The scenario described above using one measured input and one measured output is called single-channel system. As an extension, a so-called multi-channel system operates with

more than one input and output. If the LPT is carried out in multi-channel mode, all signals will be processed collectively, thereby not ignoring relations among the individual signals.

A parameter for quantifying the degree of fit between the calculated output Y_t and the measured output Z_t, i. e. the performance of the linear prediction, is the *efficiency* defined as

$$eff = \left(1 - \frac{{\sigma_r}^2}{{\sigma_z}^2}\right) \cdot 100 \qquad [\%] \tag{3}$$

${\sigma_z}^2$ is the variance of Z_t and ${\sigma_r}^2$ is the variance of the residual time series $(Z_t - Y_t)$. An efficiency of +100% means that all variations of the measured output Z_t are reproduced by the variations of the calculated output Y_t. On the other hand, a negative value for eff indicates that Y_t does not reproduce the variations of Z_t and hence the prediction of the output Z_t by the input X_t is wrong. Finally, an efficiency of exactly zero implies that the prediction yields the same results as if Y_t is just replaced by the mean of Z_t.
An exact representation of the measured output Z_t by the calculated output Y_t is only possible if the summation in equation (2) is performed from negative infinity to positive infinity and if the relation is strictly linear and time invariant. These conditions can hardly be fulfilled by real measured signals and one has to accept the fact that only a certain level of correlation lower than 100% will be achieved. So, the disadvantage of the LPT is the fact that it ignores relations having higher moments of the investigated process. Moreover, a found filter is only valid for the time period selected for the calculations. On the other hand, it simplifies the analysis as a first approximation by assuming a linear system. Even if the relation between the input and output is not strictly linear, the Linear Prediction Theory will calculate the best possible linear relation.

3 Saturn kilometric radiation and solar wind data

New data obtained by three different experiments onboard the Cassini spacecraft have been used to construct input and output signals feeding the LPT algorithm.
SKR integrated intensity-time profiles from the RPWS-experiment serve as output signals. Intensity profiles are established taking only intensities belonging to SKR emission into account. SKR emissions can be clearly identified in a dynamic spectrum regarding the frequency range and the polarization characteristics. SKR usually occurs in the frequency range 3 - 1200 kHz and exhibits a high degree of circular polarization (nearly 100%). The polarization of measured radio waves was determined by applying the Direction-Finding algorithm for a 3-axis stabilized spacecraft using a direct inversion [Cecconi and Zarka, 2005a].
Data concerning the behavior of the solar wind are monitored by the CAPS-experiment and the MAG-experiment. The latter yields measurements of the interplanetary magnetic field. The CAPS-experiment provides plasma parameters like the solar wind bulk velocity, proton density and proton temperature.
Magnetic field and plasma measurements can be combined into several other quantities describing the physical state of the solar wind and yielding additional input signals for

the LPT computations. The solar wind quantities investigated in the frame of the LPT are:

- the SW bulk velocity v and the SW ram pressure $\rho\, v^2$ [Desch and Rucker, 1983]
- the parameters $B^2\, v$ (dynamo energy flux) and $B\, v^2$ (correlates well with AKR at Earth [Gallagher and D'Angelo, 1981])
- the parameter $B_z\, v^2$ describing the erosion of planetary magnetic field lines
- the Akasofu-parameter $B^2 v\, l_0^2\, \sin^4(\theta/2)$ [Akasofu, 1978] and the modified Akasofu-parameter $B_T^2\, (v/\rho)^{1/3}\, \sin^4(\theta/2)$ [Vasyliunas et al., 1982] (θ is the polar angle in the yz-plane of the KSM-coordinate system, l_0 is a factor for the dimension of the magnetospheric cross-section and $B_T^2 = B_y^2 + B_z^2$)
- and the quantity $\frac{\mu_0\, (v_2 - v_1)^2}{B_1^2\, (1/\rho_1 + 1/\rho_2)}$ describing the probability that a Kelvin-Helmholtz instability occurs at the dayside magnetopause initiating an increased flow of charged particles into the Saturn auroral regions [Galopeau et al., 1995] (index 1 refers to parameters in the bow shock outside the magnetosphere and index 2 refers to parameters inside the magnetosphere of Saturn)

The solar wind momentum ($\rho\, v$) and the kinetic energy ($\rho\, v^3$) have not been investigated explicitly. The corresponding time profiles look very similar to the time profile of the ram pressure because variations of the density are definitely more dominant than variations of the bulk velocity.

The total time period for which data are available is limited to the period DOY $202 - 326$, 2004 due to limited availability of CAPS plasma data. Large data gaps (> 1 day) occurring after DOY 260, 2004 cannot be represented satisfactorily by interpolated values and therefore the period DOY $260 - 326$ was rejected. In the following, the results of the LPT computations found for the period DOY $224 - 240$, 2004 will be presented showing the most evident triggering effect of the solar wind on SKR. This period is centered around two clear peaks in the SKR intensity profile as can be seen in Figure 2 (solid line). Furthermore, Figure 2 displays profiles for the ram pressure (dotted line) and the bulk velocity (dashed dotted line). For the sake of clarity profiles for the other input signals are not included. Besides the modulation of SKR intensity caused by the planetary rotation, two characteristic peaks around DOY 233 are obvious. The ram pressure shows one peak at DOY 232.9 and the bulk velocity exhibits a sudden increase around DOY 231.5.

The efficiency parameter displayed as a function of the temporal shift between input and output reveals the characteristics of the linear filter found by the LPT algorithm. The efficiency functions have been established for the various input signals described above in connection with the integrated SKR intensity as output signal.
First, it was found that using the time derivative of an input quantity or the absolute value of its time derivative suppresses strong fluctuations in the efficiency function which enhances the significance.
Second, if the bulk velocity v and the magnetic field are mixed, e. g. for the dynamo energy flux $B^2\, v$ or for the erosion of magnetic field lines $B_z\, v^2$, then v seems to be of minor influence and the efficiencies of $B^2\, v$ and $B_z\, v^2$ are nearly the same as for B or B_z alone.

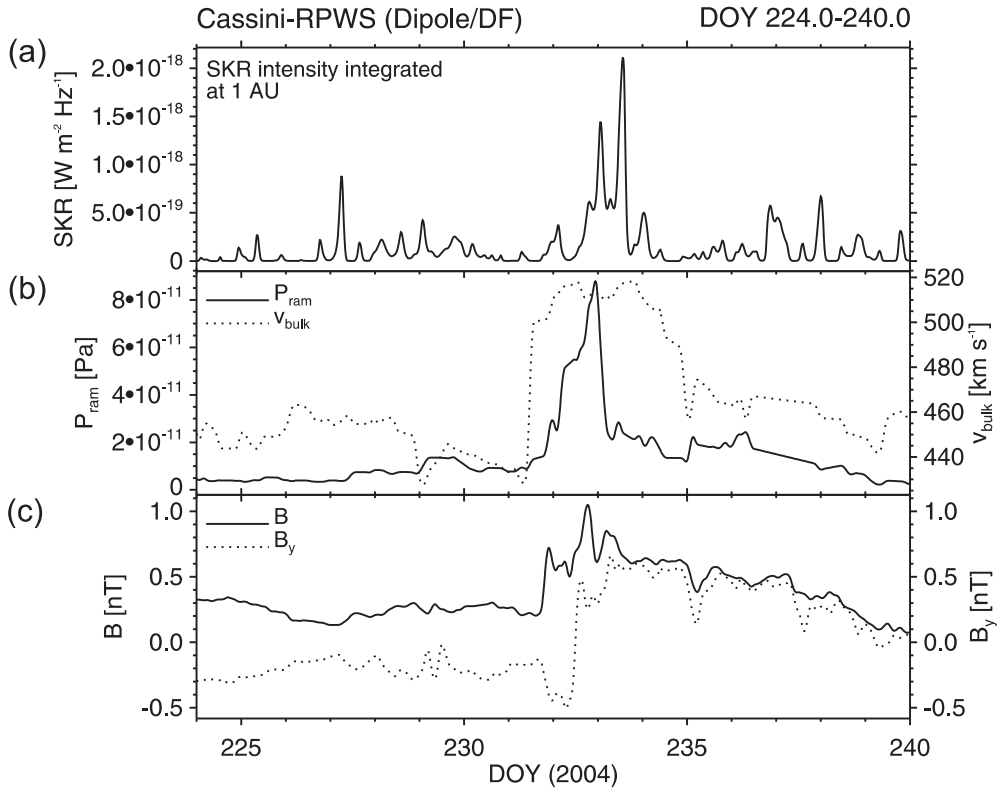

Figure 2: The integrated SKR intensity (solid line), the ram pressure (dotted line) and the bulk velocity (dashed dotted line) during DOY 224–240, 2004. Amplitude values are centered and normalized to standard deviation units.

Third, the efficiencies achieved for the proton temperature, the modified Akasofu-parameter and the instability quantity reveal no clear correlation with SKR. In comparison to the modified Akasofu-parameter, the normal Akasofu-parameter yields better results. Finally, four characteristic input signals are left yielding the best results as far the linear prediction of SKR is concerned. These four input quantities are the ram pressure P_{ram}, the bulk velocity v, the magnetic field strength B and the y-component of the magnetic field B_y given in KSM-coordinates. The respective efficiency functions for the time derivative or the absolute value of the time derivative are summarized in Figure 3.

It can clearly be seen, that the efficiency functions for P_{ram}, v and B_y exhibit significant increases in efficiency at certain temporal shifts. This implies that at these shifts the influence of variations from the inputs on variations of the output is a maximum and that these temporal shifts may be interpreted as the temporal lags required for the inputs to trigger the output. Furthermore, all four efficiency functions ,displayed in Figure 3, level off at a constant plateau level. This means that introducing larger shifts between input and output does not raise the efficiency anymore, so, the filtering between input and output is completed after a certain lag time. The characteristic lag times are $\sim (13+1)$ hours for P_{ram}, $\sim (51+1)$ hours for v, $\sim (43+1)$ hours for B and $\sim (27+1)$ hours for B_y. The additional lag time (+1) hour indicates that a characteristic solar wind structure

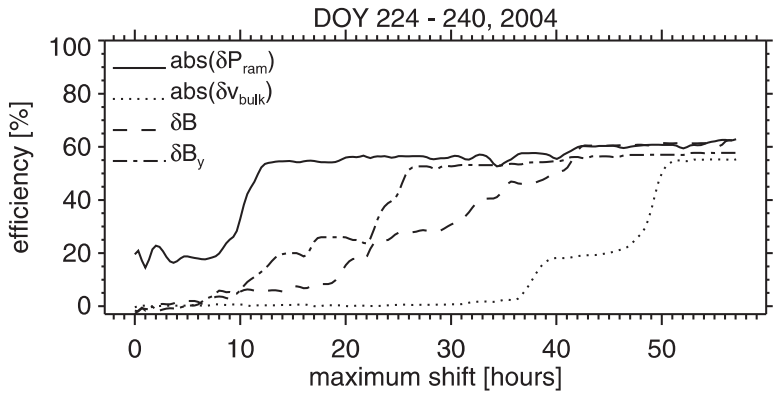

Figure 3: The efficiency as a function of the temporal shift for the ram pressure P_{ram} (solid line), the bulk velocity v (dotted line), the magnetic field strength B (dashed line) and the magnetic component B_y (dashed-dotted line). The time derivative is indicated by δ, the absolute value of the time derivative is indicated by $abs(\delta\ )$.

arrives about 1 hour earlier at the dayside magnetopause than at Cassini. This is due to the position of Cassini on its orbit around Saturn and causes an additional acausal shift for the LPT computations. During the time period $DOY\ 224 - 240$, 2004 Cassini was positioned mainly on the morning side around LT 06:00. So, e. g. for the ram pressure, it can be concluded that the physical processes involved to transform an increase in ram pressure into an increase in SKR intensity require about 14 hours.
As mentioned before, the efficiency functions for all four input quantities achieve a plateau level at $55\% - 60\%$ efficiency, so, all four input quantities seem to trigger SKR to the same degree of probability.

Finally, the cross-correlation coefficient between the ram pressure profile and the SKR intensity profile is displayed in Figure 4 to emphasize ones more the large lag times found. As can be seen, the cross-correlation yields a clear peak around 14 hours lag time.

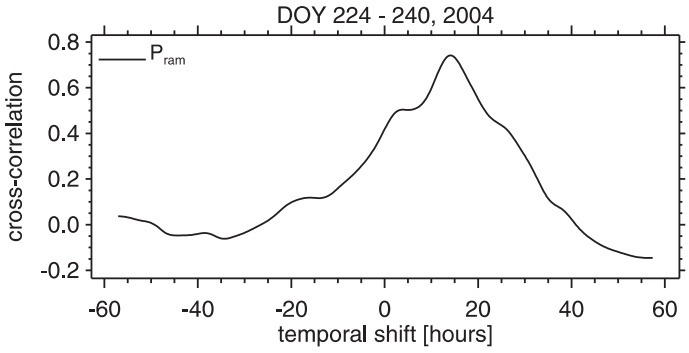

Figure 4: The cross-correlation coefficient between the ram pressure and SKR intensity as a function of the temporal shift for the period DOY 224–240, 2004.

4 Discussion and Conclusion

The conclusions drawn can be summarized as follows:

- Taking the time derivative of an input quantity or the absolute value of its time derivative enhances the efficiency function significantly. Characteristic lag times become more distinct and fluctuations of plateau levels are suppressed enabling a better interpretation.
- Four basic input signals (P_{ram}, v, B and B_y) have been found to trigger SKR with nearly the same efficiency but at completely different lag times. These lag times and efficiency levels are: $P_{ram} \rightarrow (\sim 14\,\mathrm{h},\ 55\%)$, $v \rightarrow (\sim 52\,\mathrm{h},\ 55\%)$, $B \rightarrow (\sim 44\,\mathrm{h},\ 60\%)$ and $B_y \rightarrow (\sim 28\,\mathrm{h},\ 53\%)$. For the two quantities B and B_y it may be said that the efficiency functions are more distinct if a stable sector structure for the interplanetary magnetic field is present for several days, i. e. during "quiet periods" of the interplanetary magnetic field.
- Mixing of these four quantities in the frame of a multi-channel filter does not enhance the result since included variations and lag times are too different to complement each other. The resulting efficiency function achieves very high values ($\sim 85\%$) but it does not level off at a constant plateau level before the maximum temporal shift of 57 hours is reached.
- The Akasofu-parameter yields also good results ($\sim 46\,\mathrm{h}$ lag time, 45% efficiency). The modified Akasofu-parameter, the proton temperature and the instability quantity for the Kelvin-Helmholtz instability exhibit poor correlation with SKR. So, taking the instability quantity directly as input for the linear prediction studies seems to be an insufficient approach in this respect.
- The components B_x and B_z of the interplanetary magnetic field are bad quantities for explaining the external control of SKR. The efficiency functions are either set at low levels ($\leq 25\%$) or the filtering does not seem to be completed until the maximum lag time is reached. This does not exclude the possibility that a significant influence of B_x or B_z on SKR may be found at greater lag times beyond 57 hours.
- For the output, an intensity profile integrated over frequency seems to be the best choice. As modified output signals a mean intensity, the upper frequency limit of SKR, the lower frequency limit and the frequency bandwidth have also been tested. These modifications for the output yield lower efficiencies. Especially for the outputs concerning the frequency limits, characteristic lag times are shifted to higher values. Furthermore, it was found that the efficiency function for the integrated intensity profile can be raised further if the integration is just performed from 300–1200 kHz thereby skipping intensity fluctuations which are caused by variations of the lower frequency limit. Thus, these variations seem to be rather due to the rotation of the planet than to an external influence from the solar wind.
- The integrated SKR intensity profile must be handled with care because it represents SKR activity which was beamed towards an observer, i. e. Cassini, located at a special position around Saturn. This measured profile can by no means represent SKR activity for all possible source regions which are stimulated by the solar wind.

Furthermore, slight changes in the longitude or latitude of the source region together with the hollow-cone-shaped beaming structure can cause huge intensity variations seen by a quasi-fixed distant observer [Cecconi and Zarka, 2005b].

Summarizing, it has been demonstrated that there exists a significant influence of the solar wind on the variations of SKR intensity using the Linear Prediction Theory algorithm as tool for analysis. The Linear Prediction Theory can only verify the presence of this kind of influence yielding efficiencies and lag times. The LPT is not qualified to explain why these characteristic efficiencies and lag times occur. Anyhow, this valuable information found by the LPT must be considered and explained by already existing or future model calculations dealing with the relationship between the solar wind and SKR radio emission. Further analyses may be extended to parameters including Saturn aurora phenomena like UV– and IR–measurements as has been performed by HST and ground-based observations.

References

Akasofu, S.–I., Interplanetary energy flux associated with magnetospheric substorms, *Planet. Space Sci.*, **27**, 425–431, 1978.

Cecconi, B., and P. Zarka, Direction finding and antenna calibration through analytical inversion of radio measurements performed using a system of two or three electric dipole antennas on a three–axis stabilized spacecraft, *Radio Sci.*, **40**, CiteID RS3003, 2005a.

Cecconi, B. and P. Zarka, Model of a variable radio period for Saturn, *J. Geophys. Res.*, **110**, A12203, 2005b.

Clarke, J. T., J.–C. Gérard, D. Grodent, S. Wannawichian, J. Gustin, J. Connerney, F. Crary, M. Dougherty, W. Kurth, S. W. H. Cowley, E. J. Bunce, T. Hill, and J. Kim, Morphological differences between Saturn's ultraviolet aurorae and those of Earth and Jupiter, *Nature*, **433**, 717–719, 2005.

Crary, F. J., J. T. Clarke, M. K. Dougherty, P. G. Hanlon, K. C. Hansen, J. T. Steinberg, B. L. Barraclough, A. J. Coates, J.–C. Gérard, D. Grodent, W. S. Kurth, D. G. Mitchell, A. M. Rymer, and D. T. Young, Solar wind dynamic pressure and electric field as the main factors controlling Saturn's aurorae, *Nature*, **433**, 720–722, 2005.

Desch, M. D., Evidence for solar wind control of Saturn radio emission, *J. Geophys. Res.*, **87**, 4549, 1982.

Desch, M. D., and H. O. Rucker, The relationship between Saturn kilometric radiation and the solar wind, *J. Geophys. Res.*, **88**, 8999–9006, 1983.

Desch, M. D., and H. O. Rucker, Saturn radio emission and the solar wind: Voyager-2 studies, *Adv. Space Res.*, **5**, 333–336, 1985.

Farrell, W. M., M. D. Desch, M. L. Kaiser, A. Lecacheux, W. S. Kurth, D. A. Gurnett, B. Cecconi, and P. Zarka, A nightside source of Saturn's kilometric radiation: Evidence

for an inner magnetosphere energy driver, *Geophys. Res. Lett.*, **32**, Issue 18, CiteID L18107, 2005.

Gallagher, D. L., and N. D'Angelo, Correlations between solar wind parameters and auroral kilometric radiation intensity, *Geophys. Res. Lett.*, **8**, 1087–1089, 1981.

Galopeau, P. H. M., P. Zarka, and D. Le Quéau, Source location of Saturn's kilometric radiation: The Kelvin–Helmholtz instability hypothesis, *J. Geophys. Res.*, **100**, 26397–26410, 1995.

Kaiser, M. L., M. D. Desch, J. W. Warwick, and J. B. Pearce, Voyager detection of nonthermal radio emission from Saturn, *Science*, **209**, 1238–1240, 1980.

Kaiser, M. L., M. D. Desch, W. S. Kurth, A. Lecacheux, F. Genova, B. M. Pedersen, and D. R. Evans, Saturn as a radio source, in *Saturn*, Gehrels, T. and M. S. Matthews (eds.), Univ. of Arizona Press, Tucson, 378–415, 1984.

Kurth, W. S., J. D. Sullivan, D. A. Gurnett, F. L. Scarf, H. S. Bridge, and E. C. Sittler Jr., Observations of Jupiter's distant magnetotail and wake, *J. Geophys. Res.*, **87**, 10373, 1983.

Kurth, W. S., D. A. Gurnett, J. T. Clarke, P. Zarka, M. D. Desch, M. L. Kaiser, B. Cecconi, A. Lecacheux, W. M. Farrell, P. Galopeau, J.–C. Gérard, D. Grodent, R. Prangé, M. K. Dougherty, and F. J. Crary, An Earth-like correspondence between Saturn's auroral features and radio emission, *Nature*, **433**, 722–725, 2005.

Trauger, J. T., R. E. Griffiths, J. J. Hester, J. G. Hoessel, J. A. Holtzman, J. E. Krist, J. R. Mould, R. Sahai, P. A. Scowen, K. R. Stapelfeldt, and A. M. Watson, Saturn's hydrogen aurora: wide–field planetary camera 2 imaging from the Hubble Space Telescope, *J. Geophys. Res.*, **103**, 20237–20244, 1998.

Vasyliunas, V. M., J. R. Kan, G. L. Siscoe, and S.–I. Akasofu, Scaling relations governing magnetosphere energy transfer, *Planet. Space Sci.*, **30**, 359–365, 1982.

Wiener, N., Extrapolation, interpolation, and smoothing of stationary time series with engineering applications, *Publ. Techn. Press* of the M.I.T. and John Wiley & Sons Inc., New York, 1949.

Wu, C. S., and L. C. Lee, A theory of terrestrial kilometric radiation, *Astrophys. J.*, **230**, 621–626, 1979.